Korean J. Chem. Eng., 37(5), 875-882 (2020)
DOI: 10.1007/s11814-020-0482-9

pISSN: 0256-1115
eISSN: 1975-7220

Synthesis of hollow magnetic carbon microbeads using iron oleate@alginate core-shell hydrogels and their application to magnetic separation of organic dye

Soo Young Yun*, Jun Yup Lee*, and Jaeyun Kim*,,***,****,†**

*School of Chemical Engineering, Sungkyunkwan University (SKKU), Suwon 16419, Korea
**Department of Health Sciences and Technology, Samsung Advanced Institute for Health Science & Technology (SAIHST), Sungkyunkwan University (SKKU), Suwon 16419, Korea
***Biomedical Institute for Convergence at SKKU (BICS), Sungkyunkwan University (SKKU), Suwon 16419, Korea
****Institute of Quantum Biophysics (IQB), Sungkyunkwan University (SKKU), Suwon 16419, Korea
(*Received 18 August 2019 • accepted 5 January 2020*)

Abstract−The use of biopolymers obtained from natural resources as a carbon source has attracted much attention. In this study, we introduced a novel method for synthesis of hollow magnetic carbon microbeads (HMCMs) based on core-shell alginate hydrogel microbeads consisting of a hydrophobic iron-oleate core encapsulated in a shell of ionically cross-linked alginate hydrogel using the syringe pump with the fabricated double-layered syringe needle. This allows in-situ formation of magnetic particles and carbon walls simultaneously during carbonization. After surface passivation with a silica coating followed by direct carbonization led to in-situ formation of iron oxide particles via the thermal decomposition of the iron-oleate precursor in the core region and a carbon shell derived from the cross-linked alginate polymer during carbonization. The subsequent removal of the silica shell resulted in the formation of HMCMs with a unique surface wrinkle morphology and superparamagnetic property. HMCMs were applied to remove dye from the contaminated wastewater, and the dye-adsorbed HMCMs could be easily removed by an external magnetic field. The proposed synthesis of hollow carbon microbeads can be further optimized to control the size of core-shell microbeads and the components encapsulated in the core and shell, and hence will be useful for preparing diverse types of beads for various applications.

Keywords: Syringe Pump, Carbon Microbeads, Alginate, Carbonization, Organic Dye Separation

INTRODUCTION

Synthetic dyes are used in the paper, printing, textile, cosmetics, food, and pharmaceutical industries, owing to their affordable synthesis cost, stability, and availability in various colors [1]. However, during the colorizing process, these dyes are inevitably discharged into water, not only destroying nature but also affecting human health [2-5]. Diverse approaches have been studied to purify the dye-contaminated water, such as chemical oxidation, biological treatment and physical adsorption [6]. Among these, adsorption has drawn much attention owing to its low initial operation cost and facile uses [7-10].

Carbon microbeads have received much attention due to their widespread applications in various fields, such as supercapacitors [11], lithium ion batteries [12] and adsorbents [13]. Carbon microbeads are commonly prepared by using templates like using silica template [14], zeolite [15], or block copolymers as soft templates [16]. However, templating methods usually involve complicated preparation steps and harsh environment for the synthesis, which leads researchers to focus on synthesizing carbon microbeads without using templates, such as hydrothermal method [17,18], suspension polymerization [19], microwave-assistant polycondensation [20], chemical vapor deposition [21], or pyrolysis of carbonaceous materials such as alginate hydrogel [22].

Alginate, a natural polysaccharide obtained from brown-algae, consists of mannuronic acids (M block) and gluconic acids (G block) repeating units [23]. As the G blocks in alginate can be easily crosslinked by divalent cations, such as Ca^{2+}, Ba^{2+}, or Al^{3+} to from hydrogel [24,25], alginate hydrogel has been intensively studied for diverse biomedical applications including cell encapsulation [26], drug delivery[27], and tissue engineering [28]. Recently, there have been a few reports on the use of alginate as a carbon source. The alginate, an oxygen-rich carbon precursor, was carbonized under inert gas followed by surface activation with hydrochloric acid treatment resulting a high concentration of functional groups in the carbon for electrode material for supercapacitors [29]. Fe^{3+}-crosslinked sodium alginate was pre-oxidized at 200 °C, transforming Fe(III) and alginate to Fe_2O_3 and carbon each, then material was ground into powder and calcinated under nitrogen gas to 800 °C, resulting in magnetic carbonaceous materials for removing chromium from aqueous system by adsorption [30].

However, there has been no report on the synthesis of carbon microbeads using ionically-crosslinked alginate hydrogels. As the uniform Ca^{2+}-crosslinked alginate hydrogel microbeads can be easily fabricated via electrostatic droplet generator and coaxial-needle, the carbonization of the resulting alginate microbeads would lead

†To whom correspondence should be addressed.
E-mail: kimjaeyun@skku.edu
Copyright by The Korean Institute of Chemical Engineers.

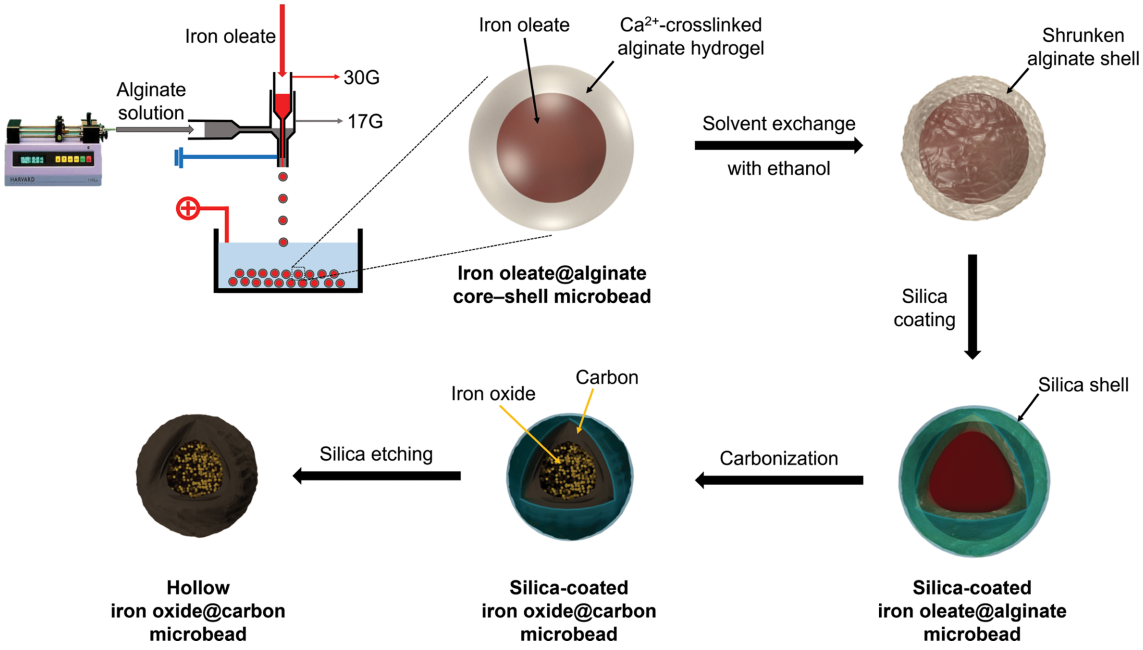


Fig. 1. Schematic of the fabrication process of hollow magnetic carbon microbeads (HMCMs) from iron-oleate@alginate core-shell microbeads.

to the preparation of uniform carbon microbeads. Furthermore, the core-shell type alginate microbeads can be designed and fabricated [26,31], which may allow functional carbon microbeads consisting of functional core part.

In this study, we propose a method for the fabrication of hollow magnetic carbon microbeads (HMCMs) based on core-shell alginate hydrogel microbeads synthesized by coaxial-needle and electrostatic droplet generator. The HMCMs were prepared via the carbonization of core-shell hydrogel microbeads consisting of iron-oleate as the hydrophobic core and Ca^{2+}-crosslinked alginate hydrogel as the shell (Fig. 1). After densification of alginate shell by solvent exchange and silica coating, the subsequent direct carbonization of iron-oleate@alginate core-shell microbeads resulted in hollow magnetic carbon microbeads (HMCMs) consisting of iron oxide nanoparticles in hollow cores and surrounding mesoporous carbon shell. The carbonization led to in-situ formation of iron oxide nanoparticles from the thermal decomposition of the iron-oleate complex and the carbon shell from the alginate layer. In general, pre-prepared magnetic nanoparticles are required to fabricate magnetic composite materials. In our study, magnetic carbon composite microbeads were fabricated directly from iron-oleate@alginate core-shell hydrogel via in-situ formation of iron oxide from decomposition of iron-oleate precursor during carbonization. Therefore, the separate preparation of magnetic nanoparticles was not necessary. The resulting hollow magnetic carbon microbeads were used for the removal of organic dyes and could be easily separated using a magnet after dye adsorption.

EXPERIMENTAL

1. Materials

An alginate acid sodium salt from brown algae with medium viscosity (Sigma), sodium chloride (Sigma-Aldrich), calcium chloride dihydrate (Sigma), poly-L-lysine (Sigma-Aldrich), tetraethyl orthosilicate (TEOS, Sigma-Aldrich), ammonium hydroxide solution (Sigma-Aldrich), sodium hydroxide (Sigma-Aldrich), iron (III) chloride hexahydrate (Sigma-Aldrich), sodium oleate (TCI), and rhodamine B (TCI) were purchased and used without further purification.

2. Preparation of Iron-oleate

Iron-oleate was prepared following the previous report [32]. Typically, 10.8 g of iron (III) chloride hexahydrate and 36.5 g of sodium oleate were dissolved in a mixture of 140 mL hexane, 80 mL ethanol, and 60 mL deionized (DI) water under stirring. The mixture was heated to 60 °C while stirring and maintained at this temperature for 4 h. After the reaction, the upper organic layer containing the iron-oleate complex was washed three times with 30 mL of DI water and EtOH in a separatory funnel, which was left overnight for the last washing step. Finally, hexane was evaporated from the retrieved organic layer in a rotary evaporator for 4 h to obtain the waxy iron-oleate complex.

3. Preparation of Core-shell Microbeads

The core-shell microbeads were prepared by co-extruding the diluted iron-oleate complex (75 wt/v% in hexane) as the core and the alginate solution (1.8 wt% in deionized water) as the shell through a specially designed blunt needle connected with a syringe pump (Pump 11 Series, Harvard Apparatus) using an electrostatic droplet generator coupled with a high-voltage power supply (13 kV, 230-30R, Bertan) [25,33]. The iron-oleate@alginate droplets were Ca^{2+}-crosslinked alginate hydrogel-based core-shell microbeads. The microbeads were spherical. The flow rates through both the inner and outer needles were adjusted to control the core and shell sizes. The core-shell microbeads were washed with 0.9 wt/v% sodium chloride (saline) solution and were then stored in for further use.

4. Preparation of the HMCMs

The core-shell microbeads were dispersed in a poly-L-lysine (PLL)

solution (0.05 wt/v% in deionized water) for 10 min and washed with saline several times, which was repeated three times. The resulting PLL-coated microbeads were dispersed in a 100 mM calcium chloride solution for a few minutes. Then, the calcium chloride solution was gradually exchanged with ethanol, which resulted in the formation of dense alginate shell via the shrinkage of hydrophilic alginate in ethanol. Subsequently, silica coating was carried out using TEOS as the silica precursor and ammonium hydroxide as the catalyst for 1 h under shaking. The resulting silica-coated microbeads were washed with ethanol several times. The silica-coated microbeads were carbonized at 900 °C for 3 h under a nitrogen atmosphere (at the heating speed of 10 °C/min). During this process, the iron-oleate complex in the core part decomposed to form iron oxide particles and the dense alginate shell converted into amorphous carbon. The obtained silica-coated carbon microbeads were incubated in a 4 M sodium hydroxide solution at 100 °C for 3 h and were then washed with excess water. The resulting HMCMs were collected and stored at room temperature.

5. Adsorption Test of Rhodamine B with the HMCMs

The adsorption of rhodamine B was tested by incubating the HMCMs (40 mg) in a 20 mL aqueous solution of rhodamine B with different concentration for different immersion durations. The adsorbed amount of rhodamine B was calculated by the following method. After magnetic separation of HMCMs, the supernatant was collected and analyzed to measure the concentration of the remaining dye using ultraviolet-visible (UV-Vis) spectroscopy at 554 nm. All the experiments were conducted at 24 °C and pH 5.0 except for the temperature and pH control.

To investigate the effect of pH and temperature on adsorption behavior, 2.5 mg of HMCMs was incubated in 0.5 mL of 5 mg/L concentration rhodamine B solution for 27 h with designed condition of pH (2.0, 5.0, 6.2, 7.0 and 9.5) and temperature (5, 24, 30 and 48 °C). To verify rhodamine B adsorption behavior in long-term adsorption, 5 mg of HMCMs was incubated at various concentrations (1.25, 2.5, 5, 10 and 20 mg/L) and at high concentration (200 mg/L) of rhodamine B solution for 7 days and 10 days, respectively, at 24 °C and pH 5.0. Isothermal tests were carried out with different concentrations (100, 50, 25, 12.5, and 6.25 mg/L) of rhodamine B at 24 °C.

RESULTS AND DISCUSSION

To prepare the core-shell microbeads consisting of a hydrophobic iron-oleate core and an alginate hydrogel shell, a double-layered syringe needle was fabricated and connected to the syringe pumps, which controlled the flow rate of the inner iron-oleate and outer alginate solutions during the droplet formation using an electrostatic droplet generator (Fig. 1). Electrostatic droplet generator applies positive charges to calcium chloride bath solution and negative charges to the tip of the syringe needle, helping microbeads to be comparably small-sized and uniform compared to syringe pump without electrostatic generator [33]. First, the core-shell microbeads consisting of an iron-oleate core and Ca^{2+}-crosslinked alginate hydrogel shell were prepared by pumping out the core-shell droplets and dropping into a calcium chloride solution, which resulted in the Ca^{2+}-crosslinking of the outer alginate shell [24,25]. The size of alginate microbeads depends on the flow rate of the inner and outer solutions, height between the needle and the accumulating pallet, and voltage of high-voltage supplier [25,33]. The thickness of core-shell microbeads depends mainly on the flow rate of the inner and outer materials (Fig. 2). When the inner flow rate was increased while maintaining the outer flow rate constant, both the core size and total size of the beads increased, but the thickness of the shell decreased (Fig. 2(a)-(d)). On the other hand, when the outer flow rate was increased while maintaining the inner flow rate constant, the total bead size and the shell thickness in-

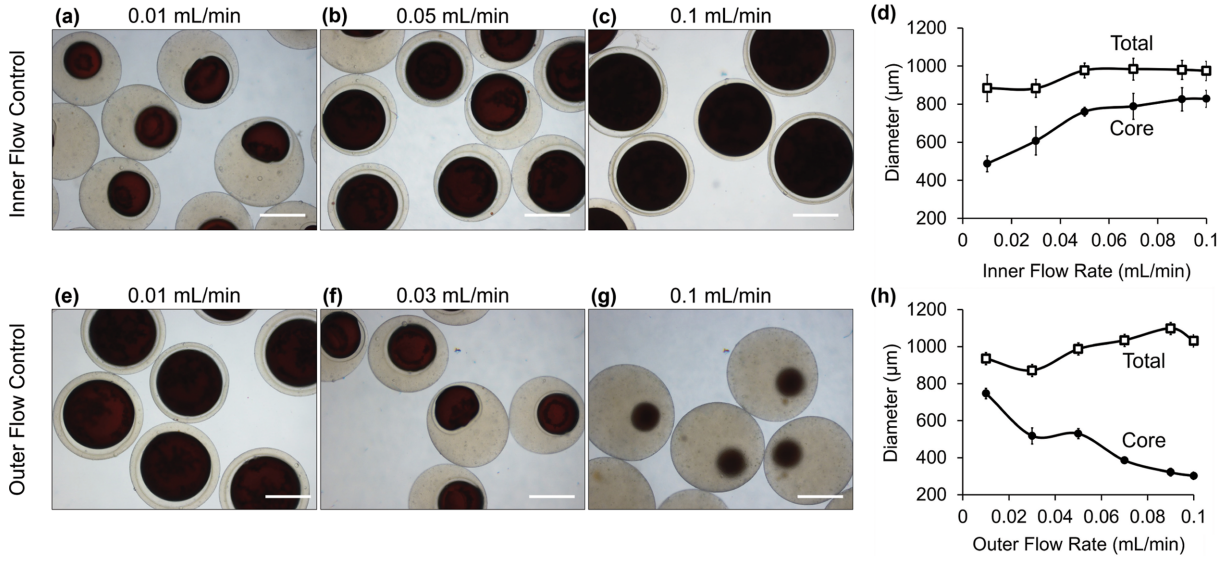


Fig. 2. Flow rate control for the double-layered microbeads. (a)-(d) Optical microscopic images (a)-(c) and the total diameter and core diameter as functions of the inner flow rate (d). The outer flow rate was fixed at 0.03 mL/min. (e)-(h) Optical microscopic images (e)-(g) and the total diameter and core diameter as functions of the outer flow rate (h). The inner flow rate was fixed at 0.01 mL/min. Scale bars: 500 μm.

creased, but the core size decreased (Fig. 2(e)-(h)). We used the inner and outer flow rates of 0.01 and 0.03 mL/min, respectively, to prepare core-shell microbeads with thicker alginate shell to increase the amount of the carbon source and encapsulate enough amount of iron-oleate to have strong magnetism for separation.

The alginate hydrogel contains low polymer contents and high water content. To densify the alginate shell, the core-shell microbeads were gradually solvent-exchanged with ethanol after coating with PLL to increase the feasibility to the silica coating. As ethanol is less polar than water, the high ethanol content around the alginate microbeads induced shrinkage of the alginate shell to form dense alginate networks because of the less solubility of hydrophilic alginate in ethanol (Fig. 3(a)). The optical microscopic images of the core-shell microbeads in saline, 50% ethanol, and 100% ethanol show that the size of the microbeads decreased significantly from 1,495 to 857 μm when the saline-to-100% ethanol solvent exchange occurred mainly due to the shrinkage of the alginate shell (Fig. 3(b)). In contrast, the size of the core did not change upon solvent exchange because hydrophobic iron-oleate was not affected by the ethanol environment. The gradual solvent exchange was important to maintain the spherical core-shell structure of the microbeads. The rapid solvent exchange from saline to 100% ethanol resulted in a distortion of the core-shell structure with the extrusion of the core material (Fig. S1).

The shrunken core-shell microbeads were coated with silica for the protection of the core-shell structure during the thermal decomposition of iron-oleate and the carbonization of the alginate shell (Fig. 3(c)). To investigate the protecting of the silica coating, the prepared silica-coated core-shell microbeads were immersed in hexane (Fig. 3(d)). The shrunken core-shell microbeads without silica coating showed a release of iron-oleate from the core as hydrophobic hexane could diffuse into the core through the alginate layer and iron-oleate could also diffuse out through the alginate shell. In contrast, the silica-coated core-shell microbeads showed no leakage of iron-oleate. Indicating that the silica coating was complete in this case and could protect the core-shell structure of

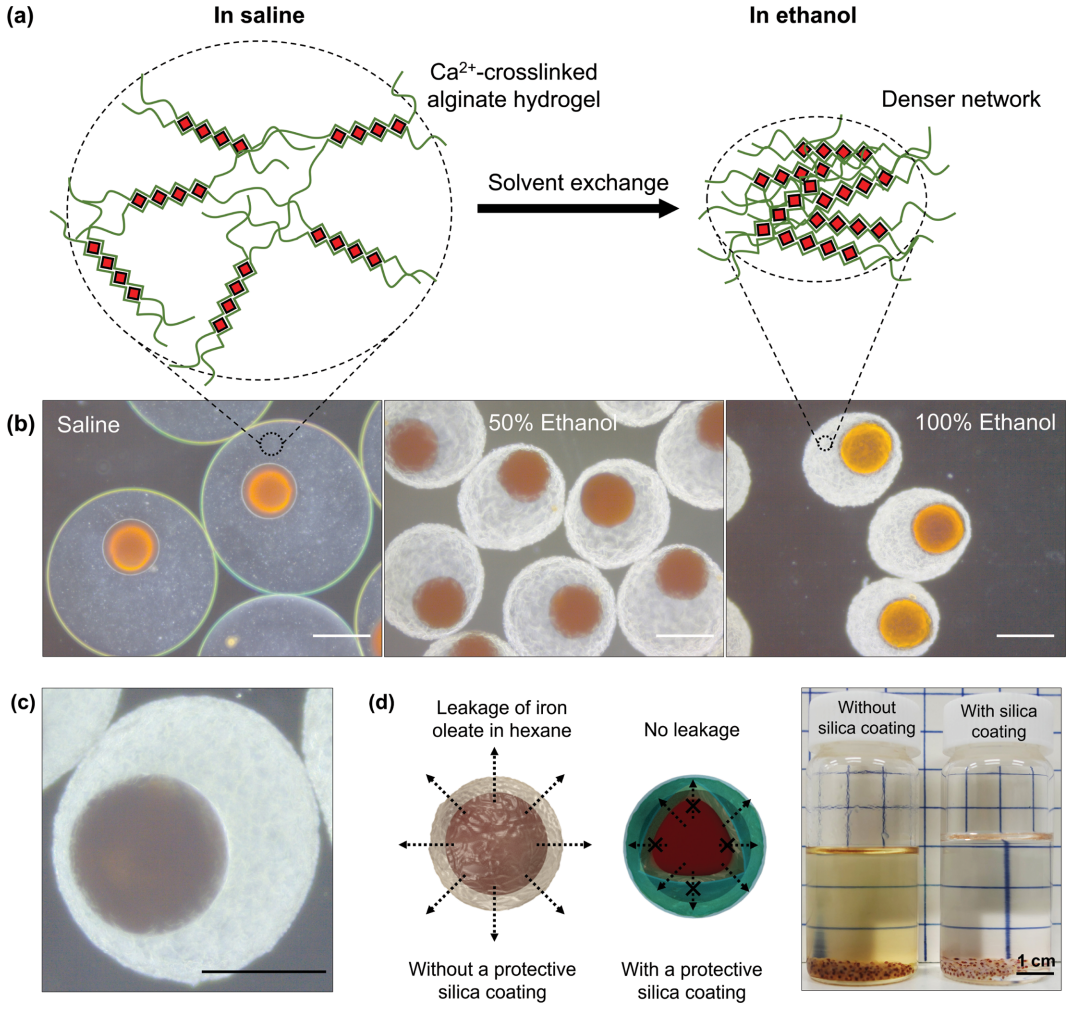


Fig. 3. Solvent exchange of the iron-oleate@alginate core-shell microbeads. (a) Schematic of the change in the distance between the alginate chains before and after the solvent exchange with ethanol. (b) Optical microscopic images of the iron-oleate@alginate core-shell microbeads over a gradual solvent exchange from saline to ethanol. Scale bars: 500 μm. (c) The representative optical microscopic image of silica-coated iron-oleate@alginate microbeads. Scale bar: 500 μm. (d) Schematic and photograph of bare iron-oleate@alginate microbeads (without silica coating) and silica-coated iron-oleate@alginate microbeads in hexane.

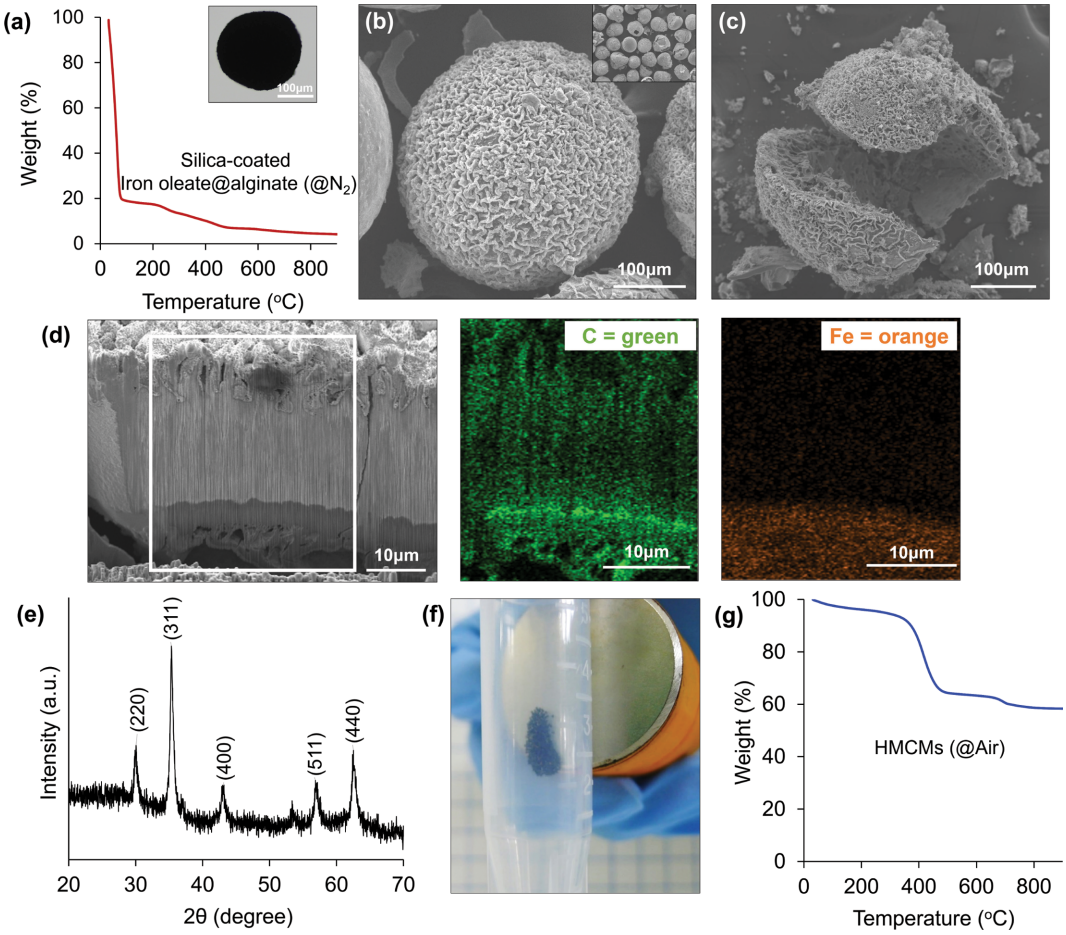


Fig. 4. Characteristics of the hollow magnetic carbon microbeads (HMCMs). (a) TGA curve for the silica-coated iron-oleate@alginate microbeads under nitrogen atmosphere (heating rate: 10 °C/min). Inset: an optical image of HMCMs after silica removal. (b) SEM image of HMCMs with densely wrinkled surfaces. (c) SEM images of the broken HMCMs revealing its hollow interior. (d) SEM image (left) and EDS mapping (C and Fe) of the broken HMCMs. (e) XRD pattern of the HMCMs with the representative diffraction peaks of iron oxide (Fe_3O_4). (f) A photograph showing the magnetic property of HMCMs. (g) TGA curve for HMCMs under air atmosphere (heating rate: 10 °C/min). (h) Isotherm sorption analysis with nitrogen gas. (i) Pore size distribution corresponding to desorption.

the microbeads by acting as the barrier for the organic solvents.

The thermal decomposition of iron-oleate complex and carbonization of alginate from the silica-coated core-shell microbeads can be demonstrated by thermogravimetric analysis (TGA) under a nitrogen atmosphere (Fig. 4(a)). The TGA graph of the silica-coated core-shell iron-oleate@alginate microbeads has four steps of weight loss upon heating. The first significant loss of weight until 80 °C is attributed to the evaporation of the solvent (ethanol and hexane) from the beads. The second weight loss at 80-200 °C is loss of water molecules which were bound between the alginate chain. The next weight loss at 200-500 °C is derived from the devolatilization along with the fracture of glycosidic bonds in alginate [34] and the decomposition of the iron-oleate complex to form iron oxide nanoparticles [32]. The last decrease of weight at 500-900 °C is from the carbonization of alginate-intermediate compounds with slow degradation [34-37].

After carbonization and the subsequent etching to remove the silica coating, black microbeads were obtained without a significant change in the morphology (Fig. 4(a) inset). The energy dispersive X-ray spectroscope (EDS) analysis of HMCMs revealed that most silica was successfully removed by etching (Fig. S2). From Fig. 4(b), it can be observed that the black microbeads were spherical and had a densely wrinkled surface. This can be attributed to the significant shrinkage of the alginate shell during the solvent exchange. The scanning electron microscopy (SEM) image of the broken microbeads shows a hollow space inside the carbon shell, which perfectly retained its structure even after the carbonization (Fig. 4(c)). The broken shell of the HMCMs was further analyzed with EDS, showing that the outer shell of the HMCMs mainly consisted of carbon while the inner surface of the microbead had an enhanced iron content (Fig. 4(d)). The X-ray diffraction (XRD) results showed that carbonization resulted in the formation of magnetite, Fe_3O_4, in the HMCMs (Fig. 4(e)). From the XRD pattern of the HMCMs, the size of the magnetite particles was estimated using the Scherrer equation, $D_{hkl}=K\lambda/(B_{hkl}\cdot\cos\theta)$, where D_{hkl} is the crystallite size in the direction perpendicular to the lattice planes, K is a numerical factor which is 0.94 for spherical crystallites with cubic symmetry, λ is the X-ray wavelength, B_{hkl} is the

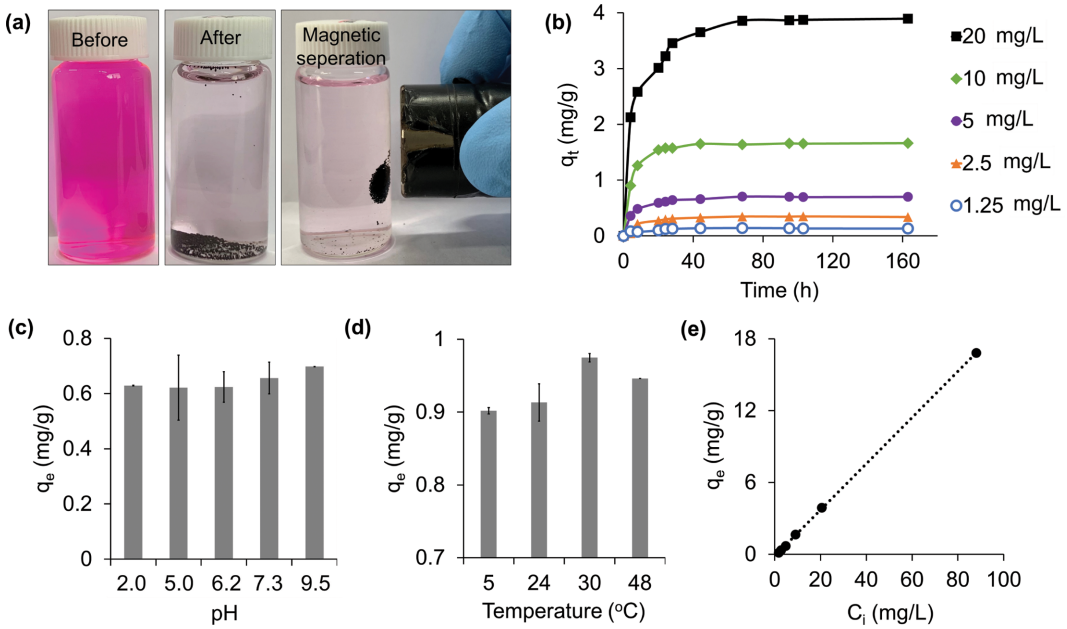


Fig. 5. Removal of rhodamine B from the aqueous solution using the HMCMs. (a) Magnetic separation of the dye-adsorbed HMCMs using a magnet. (b) Adsorption of rhodamine B with different initial concentrations over time. (c) The adsorption capacity of HMCMs depending on the initial concentration of rhodamine B. Adsorption capacity of organic dye at different (c) pH and (d) temperature. (e) Adsorption capacity of HMCMs as a function of the initial concentration of rhodamine B.

full-width at half-maximum in the XRD pattern, and θ is the Bragg angle. The Scherrer equation, often known as the Debye-Scherrer equation, explains the dependence of the crystallite size on the width of the XRD peaks to measure crystallite sizes of 200 nm or less [38]. The mean size of the magnetite particles was found to be 19.4 nm. The magnetic property of the HMCMs could be easily confirmed by applying an external magnetic field using a solid magnet (Fig. 4(f)). The magnetite content of the HMCMs was 58 wt%, as estimated from their TGA under air atmosphere in which oxygen gets to react with the carbon to produce carbon oxide or carbon dioxide with remaining inorganic iron oxide (Fig. 4(g)). In addition, porosity was investigated with nitrogen gas sorption analysis (Fig. 4(h), (i)), showing the typical hysteresis loop for the mesoporous materials. The corresponding pore size distribution showed narrow peak at 4 nm and broad peak around 10 nm. Brunauer-Emmett-Teller (BET) surface area was 157 m^2/g and average pore volume was 0.133 cm^3/g, indicating the resulting hollow magnetic carbon microbeads have meso-porosity. Taken together, the pyrolysis process followed by silica removal successfully resulted in simultaneous formation of iron oxide nanoparticles in hollow core part and carbon shell by maintaining hollow space inside the shell with mesopores [35,37].

Finally, the removal of the organic dye from contaminated water was investigated by incubating the HMCMs in an aqueous solution of rhodamine B and measuring the concentration of the remaining dye using UV-Vis spectroscopy. For adsorption analysis, rhodamine B as the organic dye material was chosen, as Rhodamine B is one of the most widely used dyes which is equally harmful towards human health like other synthetic dyes. After incubation of rhodamine B solution with HMCMs, the color of the dye solution became significantly pale and the HMCMs could be easily separated from the solution by applying an external magnetic field (Fig. 5(a)). The adsorption behavior in long-term was investigated for five different concentrations (Fig. 5(b)), showing the increase of adsorption capacity as the contact time. increased Afterwards, the adsorption became slower and reached equilibrium.

The effect of solution pH was also investigated by incubating HMCMs for 27 h at five different pH, 2.0, 5.0, 6.2, 7.0 and 9.5 of rhodamine B solution (Fig. 5(c)). There was no significant difference of dye adsorption capacity at different pH tested, suggesting the ability to remove organic dye over a wide pH range. The effect of temperature on adsorption capacity was also carried out at 5, 24, 30, and 48 °C for 27 h (Fig. 5(d)). The adsorption capacity was higher at higher temperature and maximized at 30 °C with an adsorption capacity of 0.97 mg/g. At very high temperature (48 °C) the adsorption capacity became lower. This temperature dependence was consistent with the previous reports [39,40]. Increase in temperature may generate enough energy to overcome the activation barrier for rhodamine B adsorption on HMCMs [39]. There might be an enhanced dissociation of interactions between dye and adsorbent at high temperature, resulting in lower adsorption capacity [40].

The initial organic dye concentration C_i (mg/L) versus adsorption capacity q_e (mg/g) curve of the HMCMs was obtained to evaluate their adsorption efficiency at the various initial dye concentrations (Fig. 5(e)). An increase in the initial concentration of rhodamine B led to an increase in the amount of adsorbed rhodamine B per unit weight of HMCM at equilibrium. A higher concentration of dye resulted in a higher driving force of the concentration gradient [41], which could accelerate the external diffusion of rhodamine

B molecules from the solution into the adsorbent and decrease the resistance of the uptake of rhodamine B [20,42]. As the initial concentration increased from 1.7 to 88 mg/L, the amounts of dye adsorbed on the adsorbent increased from 0.14 to 16.8 mg/g. The equilibrium between adsorbents and adsorbates can be explained by adsorption isotherms, which relate the equilibrium adsorbent capacity q_e to the equilibrium concentration of the solution C_e according to the Langmuir and Freundlich adsorption models, the most commonly used models for describing the adsorbent-adsorbate equilibrium (Fig. S3) [43-45]. The calculations revealed that the HMCMs fitted well with the Langmuir isotherm model, indicating that the HMCMs showed homogeneous sites within the adsorbent and were composed of monolayer adsorbate on the surface of the adsorbent.

CONCLUSIONS

We proposed a novel method to synthesize biomass-derived HMCMs with a tunable bead size by formation of hollow carbon microbeads and magnetite nanoparticles in hollow carbon via coaxial-needle with electrostatic droplet generator and the carbonization of core-shell microbeads consisting of an iron-oleate core and alginate hydrogel shell. The iron-oleate complex was converted into magnetite nanoparticles, and the densified alginate hydrogel shell obtained by solvent exchange was converted into carbon. These microbeads were used for the adsorption of rhodamine B in an aqueous solution. It was found that the HMCMs could remove around 80% of the dye from the aqueous solution. The dye adsorbed HMCMs could be easily separated from the solution. As the HMCMs followed the Langmuir isotherm model, they had a monolayer adsorption onto the surface containing a finite number of identical sites. The synthesis method proposed in this study can be used to prepare core-shell microbeads with various compositions, geometries, core sizes, shell thicknesses, and number of cores for various applications like lithium ion battery, desalination and energy storage system.

ACKNOWLEDGEMENT

This work was supported by the Basic Science Research Program through the National Research Foundation (NRF) funded by the Ministry of Science and ICT, Republic of Korea (2010-0027955, 2019R1A2C2004765).

SUPPORTING INFORMATION

Additional information as noted in the text. This information is available via the Internet at http://www.springer.com/chemistry/journal/11814.

REFERENCES

1. M. Arami, N. Y. Limaee, N. M. Mahmoodi and N. S. Tabrizi, *J. Colloid Interface Sci.*, **288**, 371 (2005).
2. T. Robinson, B. Chandran and P. Nigam, *Water Res.*, **36**, 2824 (2002).
3. M. Mohammadi, A. J. Hassani, A. R. Mohamed and G. D. Najafpour, *J. Chem. Eng. Data*, **55**, 5777 (2010).
4. H. Liu, X. Ren and L. Chen, *J. Ind. Eng. Chem.*, **34**, 278 (2016).
5. M. T. Yagub, T. K. Sen, S. Afroze and H. M. Ang, *Adv. Colloid Interface Sci.*, **209**, 172 (2014).
6. T. Robinson, G. McMullan, R. Marchant and P. Nigam, *Bioresour. Technol.*, **77**, 247 (2001).
7. G. Crini, *Bioresour. Technol.*, **97**, 1061 (2006).
8. T. A. Saleh and I. Ali, *J. Environ. Chem. Eng.*, **6**, 5361 (2018).
9. V. Katheresan, J. Kansedo and S. Y. Lau, *J. Environ. Chem. Eng.*, **6**, 4676 (2018).
10. G. San Miguel, S. D. Lambert and N. J. D. Graham, *J. Chem. Technol. Biotechnol.*, **81**, 1685 (2006).
11. H. Kim, M. E. Fortunato, H. Xu, J. H. Bang and K. S. Suslick, *J. Phys. Chem. C*, **115**, 20481 (2011).
12. Y. Wang, L. Zhang, Y. Wu, Y. Zhong, Y. Hu and X. W. Lou, *Chem. Commun.*, **51**, 6921 (2015).
13. S. Olivera, K. Venkatesh, N. Reddy, B. K. Jayanna, Inamuddin, A. M. Asiri, S. Rtimi and H. B. Muralidhara, *Environ. Technol. Innovation*, **12**, 160 (2018).
14. J. Galán, A. Rodríguez, J. M. Gómez, S. J. Allen and G. M. Walker, *Chem. Eng. J.*, **219**, 62 (2013).
15. L. Tosheva, J. Parmentier, V. Valtchev, C. Vix-Guterl and J. Patarin, *Carbon*, **43**, 2474 (2005).
16. J. Liu, T. Yang, D.-W. Wang, G. Q. Lu, D. Zhao and S. Z. Qiao, *Nat. Commun.*, **4**, 2798 (2013).
17. M. Li, Q. Wu, M. Wen and J. Shi, *Nanoscale Res. Lett.*, **4**, 1365 (2009).
18. X. Wang, C. Jiang, B. Hou, Y. Wang, C. Hao and J. Wu, *Chemosphere*, **206**, 587 (2018).
19. L. Ding and S. V. Olesik, *Chem. Mater.*, **17**, 2353 (2005).
20. F. Lu, C. Huang, L. You, J. Wang and Q. Zhang, *RSC Adv.*, **7**, 23255 (2017).
21. H.-S. Qian, F.-M. Han, B. Zhang, Y.-C. Guo, J. Yue and B.-X. Peng, *Carbon*, **42**, 761 (2004).
22. T. Zhang, C. Zhu, Y. Shi, Y. Li, S. Zhu and D. Zhang, *Mater. Lett.*, **205**, 10 (2017).
23. M. S. Shoichet, R. H. Li, M. L. White and S. R. Winn, *Biotechnol. Bioeng.*, **50**, 374 (1995).
24. Ý. A. Mørch, I. Donati and B. L. Strand, *Biomacromolecules*, **7**, 1471 (2006).
25. B. P. Barnett, A. Arepally, M. Stuber, D. R. Arifin, D. L. Kraitchman and J. W. M. Bulte, *Nat. Protocols*, **6**, 1142 (2011).
26. J. Kim, D. R. Arifin, N. Muja, T. Kim, A. A. Gilad, H. Kim, A. Arepally, T. Hyeon and J. W. M. Bulte, *Angew. Chem. Int. Ed.,* **50**, 2317 (2011).
27. B. Y. Shin, B. G. Cha, J. H. Jeong and J. Kim, *ACS Appl. Mater. Interfaces*, **9**, 31372 (2017).
28. X. Yang, Z. Lu, H. Wu, W. Li, L. Zheng and J. Zhao, *Mater. Sci. Eng.: C*, **83**, 195 (2018).
29. E. Raymundo-Piñero, F. Leroux and F. Béguin, *Adv. Mater.*, **18**, 1877 (2006).
30. Z. Lei, S. Zhai, J. Lv, Y. Fan, Q. An and Z. Xiao, *RSC Adv.*, **5**, 77932 (2015).
31. K. Cho, B. Y. Shin, H. K. Park, B. G. Cha and J. Kim, *RSC Adv.*, **4**, 21777 (2014).

32. J. Park, K. An, Y. Hwang, J.-G. Park, H.-J. Noh, J.-Y. Kim, J.-H. Park, N.-M. Hwang and T. Hyeon, *Nat. Mater.*, **3**, 891 (2004).
33. K.-S. Huang, C.-H. Yang, Y.-S. Lin, C.-Y. Wang, K. Lu, Y.-F. Chang and Y.-L. Wang, *Drug Deliv. and Transl. Res.*, **1**, 289 (2011).
34. F. Guerretta, G. Magnacca, F. Franzoso, P. Ivanchenko and R. Nisticò, *Mater. Lett.*, **234**, 339 (2019).
35. A. B. Ross, C. Hall, K. Anastasakis, A. Westwood, J. M. Jones and R. J. Crewe, *J. Anal. Appl. Pyrol.*, **91**, 344 (2011).
36. D. Li, L. Chen, X. Yi, X. Zhang and N. Ye, *Bioresour. Technol.*, **101**, 7131 (2010).
37. J. P. Soares, J. E. Santos, G. O. Chierice and E. T. G. Cavalheiro, *Eclética Química*, **29**, 57 (2004).
38. U. Holzwarth and N. Gibson, *Nat. Nanotechnol.*, **6**, 534 (2011).
39. K. G. Bhattacharyya, S. Sengupta and G. K. Sarma, *Appl. Clay Sci.*, **99**, 7 (2014).
40. A. A. Inyinbor, F. A. Adekola and G. A. Olatunji, *S. Afr. J. Chem.*, **69**, 218 (2016).
41. S. Chaudhary, P. Sharma, Renu and R. Kumar, *RSC Adv.*, **6**, 62797 (2016).
42. S. K. Giri, N. N. Das and G. C. Pradhan, *Colloids Surf. A: Physicochem. Eng. Aspects*, **389**, 43 (2011).
43. A. Sinha, B. G. Cha and J. Kim, *ACS Appl. Nano Mater.*, **1**, 1940 (2018).
44. M. Santhi and P. E. Kumar, *Int. J. Innov. Res. Sci. Eng. Technol.*, **4**, 497 (2015).
45. X. Pan, Q. Du, Y. Zhou, L. Liu, G. Xu and C. Yan, *J. Nanosci. Nanotechnol.*, **18**, 7231 (2018).

Supporting Information

Synthesis of hollow magnetic carbon microbeads using iron oleate@alginate core-shell hydrogels and their application to magnetic separation of organic dye

Soo Young Yun*, Jun Yup Lee*, and Jaeyun Kim*,,***,****,†**

*School of Chemical Engineering, Sungkyunkwan University (SKKU), Suwon 16419, Korea
**Department of Health Sciences and Technology, Samsung Advanced Institute for Health Science & Technology (SAIHST), Sungkyunkwan University (SKKU), Suwon 16419, Korea
***Biomedical Institute for Convergence at SKKU (BICS), Sungkyunkwan University (SKKU), Suwon 16419, Korea
****Institute of Quantum Biophysics (IQB), Sungkyunkwan University (SKKU), Suwon 16419, Korea
(*Received 18 August 2019 • accepted 5 January 2020*)

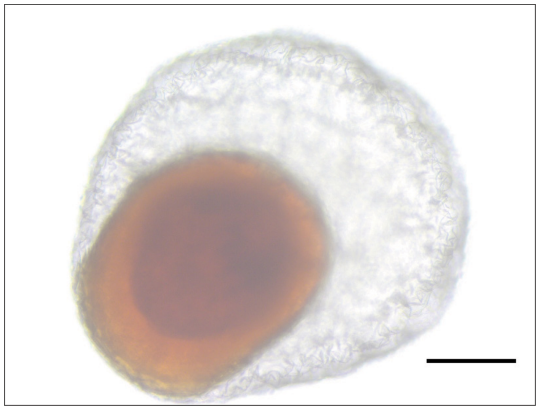
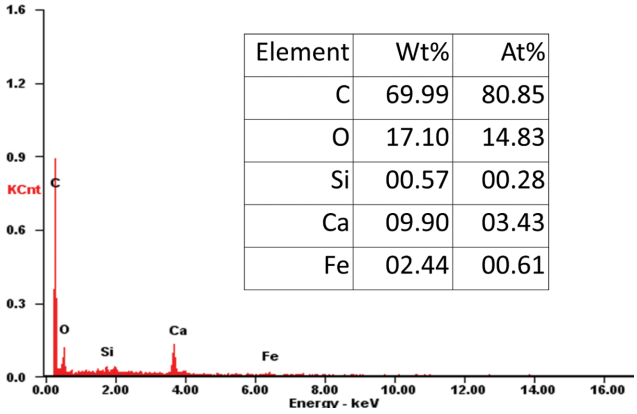


Fig. S1. Shape maintenance of the HMCMs with radical solvent exchange. Scale bar: 200 μm.

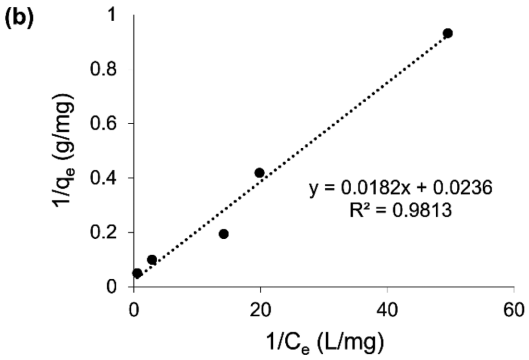


Element	Wt%	At%
C	69.99	80.85
O	17.10	14.83
Si	00.57	00.28
Ca	09.90	03.43
Fe	02.44	00.61

Fig. S2. EDS elemental analysis of HMCMs, revealing the successful removal of silica after etching.

(a)

	Langmuir			Freundlich		
	K_L (L/mg)	q_L (mg/g)	R^2	K_F (L/mg)	n	R^2
rhodamine B	1.297	42.372	0.981	16.260	1.633	0.923



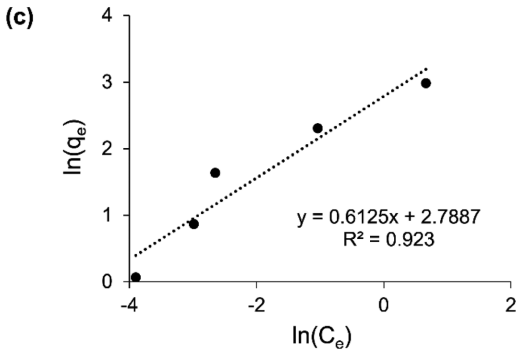


Fig. S3. (a) Parameters for the adsorption isothermal models. (b) Langmuir model: $1/q_e$ vs. $1/C_e$. (c) Freundlich model: $\ln(q_e)$ vs. $\ln(C_e)$.